Published in final edited form as:
Annu Rev Biophys. 2014 ; 43: 303–329. doi:10.1146/annurev-biophys-051013-022836.

Photocontrollable Fluorescent Proteins for Superresolution Imaging

Daria M. Shcherbakova[1,2], **Prabuddha Sengupta**[3], **Jennifer Lippincott-Schwartz**[3], and **Vladislav V. Verkhusha**[1,2]

Jennifer Lippincott-Schwartz: lippincj@mail.nih.gov; Vladislav V. Verkhusha: vladislav.verkhusha@einstein.yu.edu

[1]Department of Anatomy and Structural Biology, Albert Einstein College of Medicine, Bronx, New York 10461

[2]Gruss-Lipper Biophotonics Center, Albert Einstein College of Medicine, Bronx, New York 10461

[3]Section on Organelle Biology, Cell Biology and Metabolism Program, Eunice Kennedy Shriver National Institute of Child Health and Human Development, National Institutes of Health, Bethesda, Maryland 20892

Abstract

Superresolution fluorescence microscopy permits the study of biological processes at scales small enough to visualize fine subcellular structures that are unresolvable by traditional diffraction-limited light microscopy. Many superresolution techniques, including those applicable to live cell imaging, utilize genetically encoded photocontrollable fluorescent proteins. The fluorescence of these proteins can be controlled by light of specific wavelengths. In this review, we discuss the biochemical and photophysical properties of photocontrollable fluorescent proteins that are relevant to their use in superresolution microscopy. We then describe the recently developed photoactivatable, photoswitchable, and reversibly photoswitchable fluorescent proteins, and we detail their particular usefulness in single-molecule localization–based and nonlinear ensemble–based superresolution techniques. Finally, we discuss recent applications of photocontrollable proteins in superresolution imaging, as well as how these applications help to clarify properties of intracellular structures and processes that are relevant to cell and developmental biology, neuroscience, cancer biology and biomedicine.

Keywords

PALM; RESOLFT; PAGFP; PAmCherry; EosFP

INTRODUCTION

Optical imaging using genetically encoded fluorescent proteins (FPs) is arguably the most widely used approach for noninvasive studies of biological processes at different scales

DISCLOSURE STATEMENT

The authors are not aware of any affiliations, memberships, funding, or financial holdings that might be perceived as affecting the objectivity of this review.

(from molecules to organisms). Because of light's diffraction limit, however, the inherent nature of light microscopy limits its ability to visualize objects with sizes smaller than 200 nm in the lateral direction and 500 nm in the axial direction. This poses a problem for imaging small, abundant subcellular structures that have sizes in the tens of nanometer range. To overcome this obstacle, several superresolution imaging techniques have been invented (6, 29, 35, 36, 63). These techniques make it possible to obtain images with exquisite spatial resolution and therefore are now widely used by researchers.

FPs enable straightforward and specific labeling of cells without a need to deliver any additional substances. Modern FPs are available in various forms. In this review, we focus on light-controllable FPs whose fluorescence is regulated by light irradiation of specific wavelengths. These FPs can be classified into three forms: photoactivatable FPs (PAFPs), photoswitchable (also called photoconvertible) FPs (PSFPs), and reversibly photoswitchable FPs (rsFPs). PAFPs undergo activation from a nonfluorescent (dark) state to a fluorescent state, whereas PSFPs can be converted from one fluorescent state (or "color") to another. In contrast to PAFPs and PSFPs, which can be photoconverted only once, rsFPs can be photoswitched repeatedly between fluorescent and nonfluorescent states. We refer to these light-controllable FPs as photocontrollable FPs. Although the brightness, photostability, and photoactivation characteristics of organic dyes and other fluorophores can be superior to those of photocontrollable FPs, these substances require sophisticated approaches to increase labeling specificity and to deliver them to biological cells. The simplicity and specificity of labeling proteins of interest with photocontollable FPs have made these proteins increasingly popular tools for superresolution imaging.

In recent years, the engineering of new photocontrollable FPs has been spurred by their applicability to superresolution microscopy. As a result, researchers may now choose among many photocontrollable FPs. The optimal choice depends on the particular imaging technique. All photocontollable FP-based superresolution methods image fluorophores separately over time by controllably turning them on and off. Two strategies have been employed to construct a superresolution image (Figure 1). One strategy is based on localizing individual fluorophore molecules through cycles of stochastic activation of a small subset of photocontrollable FPs in a densely labeled structure (6, 36). This approach was first demonstrated in the similar techniques called photoactivated localization microscopy (PALM) (6), fluorescence PALM (36) and stochastic optical reconstruction microscopy (63), and has been expanded to include different single molecule–based PALM variations. The second strategy uses nonlinear optical approaches (29, 35) to reduce the spot size of an ensemble of excited photocontrollable FPs (38). This technique is called reversible saturatable optical fluorescence transition (RESOLFT) imaging.

In this review, we survey photocontrollable FPs and their uses in PALM and RESOLFT superresolution imaging techniques. For an in-depth description of other superresolution techniques we refer readers to the recent reviews (33, 43, 57). We first discuss the conceptual bases of the two superresolution imaging strategies, highlighting critical parameters important for each strategy to work. We then review modern photocontrollable FPs, along with their advantages and limitations for use in superresolution microscopy.

Finally, we consider how PALM and RESOLFT superresolution imaging have helped clarify different biological questions.

OPERATIONAL PRINCIPLES OF PHOTOCONTROLLABLE PROTEIN-BASED SUPERRESOLUTION TECHNIQUES

Conceptual Basis of Photoactivated Localization Microscopy (PALM) and Related Single-Molecule Techniques

The development of advanced microscopy instrumentation has now made detection of a single fluorescent protein possible (46). The focused emission from a single protein molecule produces a diffracted, blurred spot with an intensity profile represented by the point-spread function (PSF) of the microscope. For high numerical aperture (NA) lenses and visible light, the size of this spot is approximately 200 × 500 nm in the lateral and axial dimensions, respectively. The intensity profile of this spot (i.e., the PSF) can be fitted with a two-dimensional Gaussian, and its center can be localized to within tens of nanometers (82).

Because the image produced by a single molecule is distended (i.e., a blurred spot), fluorescing protein molecules present within a distance less than the dimension of this spot (i.e., the diffraction limit) cannot be distinguished because their individual images are merged. However, if one can ensure that simultaneously fluorescing FPs are spread further from each other than this diffraction-limited distance, each FP can be individually localized. PALM exploits this concept. This technique achieves an appropriate separation distance between fluorescing molecules via stochastic activation of small subsets of photocontrollable FPs within a densely labeled structure using low-intensity light (Figure 1*a–c*) (6, 36, 63). The activated molecules are imaged, localized, and then deactivated by permanent photobleaching or by turning the fluorescence off. This process is repeated thousands of times to accumulate millions of molecular positions. This imaging concept has been implemented using total internal reflection fluorescence (6) and epifluorescence (36, 63) imaging geometries, as well as using photocontrollable FPs (6, 36) and synthetic dyes (63). All types of photocontrollable FPs, such as PAFPs, PSFPs and rsFPs, are suitable for single-molecule based superresolution imaging.

Resolution of Photoactivated Localization Microscopy (PALM) and Related Single-Molecule Techniques

The spatial resolution of single-molecule superresolution microscopy depends on how well the individual molecules are localized and how densely they are localized in a labeled structure. The accuracy of localization is equivalent to the precision, such as standard deviation, with which the center of a single FP image (i.e., the diffraction spot) can be determined by mathematical fitting (Figure 2*a*). The value of this localization precision (σ) scales with the inverse square root of the number of detected photons (82). A full-width half maximum (FWHM) of an intensity profile can characterize the spatial resolution. For a Gaussian distribution, the FWHM approximately corresponds to 2.355 σ. The experimentally measured localization precision is often worse than the theoretically predicted value (Figure 2*b*).

The density of localized molecules critically influences the spatial resolution (57) because at least two proteins must be localized across the smallest unit of resolution in a superresolution image (Figure 2*c*). This requirement, formulized by the Nyquist–Shannon sampling theorem (67), sets an upper limit to the resolution that can be attained in PALM using photocontrollable FPs with a size of approximately 2.5 nm and a limited labeling density. Typical single-molecule densities vary in the range of 10^3–10^5 molecules per square micrometer, which corresponds to a maximum achievable resolution of 6–48 nm (54).

As discussed above, PALM and related techniques sequentially acquire up to tens of thousands of raw images, each containing a small subset of fluorescing molecules. This limits the acquisition speed and the ability of a technique to image dynamic processes, decreasing the temporal resolution. Recently, several PALM techniques using rsFPs have been developed, allowing faster acquisition speed. One such technique is PALM with independently running acquisition (PALMIRA) (18), which utilizes spontaneous off-on-off cycles of an rsFP without synchronization to a detector. The same light of selected intensity is used to stochastically switch off the majority of molecules, leaving a small subset in the on state, and to excite these remaining sparsely distributed molecules. PAFPs and PSFPs can also be used in PALMIRA, provided that the activation and imaging illuminations are continuously on. In another such technique, called stroboscopic PALM (s-PALM) (19), a two-color illumination is applied. Continuous light is used for switching off fluorophores and for excitation, and pulsed activating light is used for switching the rsFP molecules to the on state. However, faster acquisition time in these techniques comes at the cost of resolution due to the low number of acquired photons per cycle. rsFPs have been also applied to photochromic stochastic optical fluctuation imaging (pcSOFI), a single-molecule imaging technique that analyzes the statistics of temporal fluctuations of fluorescence pixel-by-pixel without localization of molecules (16). pcSOFI is characterized by easy technical implementation and a high speed of data acquisition.

Conceptual Basis and Resolution of Reversible Saturatable Optical Fluorescence Transition (RESOLFT) and Related Ensemble Techniques

The ensemble-based superresolution imaging approaches are based on an optically driven saturatable transition of rsFPs between a fluorescent and a dark state. A patterned beam of light is used to illuminate the sample in a nonlinear fashion, confining a fluorescent diffraction-limited spot (29, 35).

Two strategies can be used to achieve spatial light modulation in order to confine a fluorescent diffraction-limited spot. In one, a structured illumination microscopy (SIM) approach called saturated SIM (SSIM) (29), the sample is illuminated by patterned excitation light obtained by combining two interfering light beams. The pattern is scanned and rotated, after which the resulting images are combined to obtain a final image. In a second approach, stimulated emission depletion (STED) microscopy, the doughnut-like beam suppresses the fluorescence of molecules in a focal spot of the excitation laser via photon-induced deexcitation (35). Scanning the two beams across the sample and recording fluorescence produces the resulting image. The STED beam uses light intensities that are above FP saturation levels (32). These high intensities are needed to increase the probability

of photons interacting with fluorophores in the short time corresponding to the lifetime of the excited state. The diameter of the confined fluorescent spot scales approximately with the inverse square root of the STED beam intensity (33). Typically, light intensities of ~100 MW/cm^2 are required to reach a resolution of 40 nm (34); such high intensities can be damaging to biological samples. To reduce the required light intensities, other transitions between fluorophore states have been utilized. In ground-state depletion (GSD) imaging, for example, the fluorophores are switched off by a transient transfer to the generic metastable dark (triplet) state, allowing lower-intensity light to be used (20). Note that SSIM, STED, GSD, and their modifications typically utilize permanently fluorescent FPs.

Recently, patterned illumination techniques have advanced towards live-cell imaging using comparatively low light intensities. A STED-like approach known as RESOLFT depletes the overall fluorescence by switching rsFPs between their fluorescent and dark states (Figure 1*d–f*) (32). The nonlinear technique SIM has also been adapted for use with low light intensities and rsFPs as probes (60)

Spatial resolution in RESOLFT and other patterned illumination techniques can be characterized by FWHM of the intensity profile, which corresponds to a cellular structure (Figure 3*a*). To obtain enough data points to satisfy the Nyquist criterion of resolution (66, 67), the scanning step should be smaller than half the desired resolution (Figure 3*b*). The resolution possible in RESOLFT and similar patterned light illumination techniques sets strong requirements for rsFPs. Earlier imaging beyond the proof of principle (15, 38) was not possible because the early rsFPs bleached quickly. The three overlaid beams for switching on, switching off, and exciting fluorescence scan the sample, so the same rsFP molecules have to withstand many cycles of photoswitching to obtain high resolution (Figure 3*c*). As an estimate, to reach a tenfold increase in resolution, the probes must be switched 100 times for two-dimensional imaging and 1,000 times for three-dimensional (3D) imaging, with no loss of fluorescent signal (34). One study demonstrated that a fatigue resistance of more than 1,000 switching cycles before bleaching to 50% is compatible with RESOLFT imaging of live mammalian cells (25).

PHOTOCONTROLLABLE FLUORESCENT PROTEINS AS TOOLS FOR SUPERRESOLUTION MICROSCOPY

Photophysical and Biochemical Properties of Photocontrollable Fluorescent Proteins

Superresolution imaging involves photomanipulation of photocontrollable protein molecules. PALM imaging of single molecules requires consideration of their unique photophysical and biochemical properties, which are often overlooked in ensemble microscopy techniques. As discussed above, during a PALM experiment, individual PAFP and PSFP molecules undergo a sequence of three distinct events: photoconversion, fluorescence emission, and photobleaching. The optimal implementation of PALM depends critically on the tight modulation of these three processes. Because the photophysical properties of a single photocontollable FP molecule that influences these processes determine the number of FPs detected, as well as their precision of their localization, these properties thereby determine the final resolution of the PALM image. In contrast, other

specific photophysical properties of rsFPs are required to obtain high resolution in RESOLFT. rsFP molecules used for RESOLFT should be characterized by a fatigue resistance high enough to withstand many cycles of photoswitching using light of intensities high enough to considerably saturate most of the molecules in the diffraction-limited spot. Below, we discuss properties of photocontrollable FPs that affect their performance in PALM and RESOLFT.

Properties affecting single-molecule localization—The number of photons collected from a single FP determines both the probability of successfully detecting it and the localization accuracy of such a detection (Figure 2). Thus, factors affecting the number of photons emitted by an FP critically influence performance of PALM. One such key factor is the brightness of a single FP, which is a measure of the number of photons emitted per second by the FP. This molecular brightness depends on single-molecule properties such as the excitation cross-section, the quantum efficiency of emission, and the photon emission rate. The single-molecule brightness of an FP can have a value higher than that of the corresponding ensemble (73) when nonproductive transitions into dark states compete with fluorescence emission, thereby decreasing the average brightness value. Besides the molecular brightness, the total number of photons emitted per molecule before photobleaching (i.e., the photon budget) also influences the photon number.

Undesirable reversible and irreversible light-induced and thermal transitions also affect the detection and localization accuracy of individual FPs. In single-molecule localization techniques, spontaneous blinking of fluorophore molecules (17) is a notable problem (64). Blinking and other nonproductive competing fluorophore transitions into nonfluorescent states influence the quantum yield of photoconversion, which corresponds to the probability that a molecule will undergo photoactivation upon an absorption of a photon. FP blinking may decrease the number of photons collected, which can hamper the detection of single FPs and degrade their localization accuracy. This phenomenon may also complicate the precise localization of single molecules, as blinking molecules may be counted and localized several times, and fluorescence may be detected from several molecules that are not separated by a distance larger than the diffraction spot.

Another important parameter is photoactivation contrast (43, 57, 65), which is determined from the increase in fluorescence signal among molecules in the photoconverted state (Figure 2). This parameter depends on the rate of photon emission in the photoactivated state, the level of residual emission in the dark state, and a probability of spontaneous thermal activation. Photoactivation contrast is crucial in single-molecule imaging, in which relatively high background autofluorescence can interfere with the detection of single molecules. Higher photoactivation contrast results in the collection of larger numbers of photons over the background signal, facilitating the detection of single FPs and increasing the localization precision of the photocontrollable FPs.

The photoswitching rate is an important parameter in both single-molecule and ensemble superresolution imaging. Ideally, this rate should allow fast enough photoactivation that low light intensities can be used, with minimal spontaneous thermal activations. However, photoswitching on rates should be slow enough to allow controlled photoconversion without

overcrowding photoconverted molecules. In addition, rsFPs that exhibit slow switching off rates enable collecting a sufficient number of photons per molecule.

Properties affecting density of localized molecules—The density of localized molecules in a labeled structure is influenced by labeling density and the number of molecules undergoing activation, which correlates with the quantum yield of photoconversion and the photoactivation contrast. Poor labeling density may result from inefficient protein maturation. In addition, the density of localized molecules depends on the photon budget because there is a distribution of total photon numbers emitted by all the molecules and because the specific localization precision sets a threshold for including the molecules in the analysis. One can exclude dim molecules with low signal-to-background ratios and low localization precision from the analysis, but doing so results in a loss of resolution according to the Nyquist criterion. Consequently, a higher value of photoactivation contrast contributes to enhanced image resolution by increasing both the number of molecules localized and their average localization precision.

Properties affecting fatigue resistance—The photoswitching rate of rsFPs affects their fatigue resistance, defined as their ability to be switched multiple times without loss of brightness. As discussed above, this is an important parameter in ensemble superresolution techniques, such as RESOLFT, that involve multiple photoconversion events of rsFPs between bright and dark states (Figure 3). Faster switching rates enable rsFPs to undergo more photoswitching cycles (26) because the per-cycle light dose is lower. However, there is a trade-off between the length of a photoswitching cycle and signal-to-background ratio. The fatigue resistance also depends on the excitation light intensity, irradiation setup, imaging conditions, and illumination time in each cycle.

Biochemical properties—The process of folding and chromophore formation, also called maturation, depends on the nature of the chromophore, the oxygen concentration, and the temperature. This process can take from a few minutes to several hours. FPs that mature efficiently and quickly at 37°C perform better in protein fusions. Also, the oligomeric state and size of FPs are the critical parameters for protein labeling. In most protein fusions, an FP must be monomeric, as oligomerization would otherwise interfere with the function and localization of the fusion partner, especially at a high local concentration (87). Substantial molecular engineering efforts (28, 31, 54, 77) were required to develop monomeric photocontrollable FPs from naturally occurring FPs, most of which are tetramers or dimers (12, 77). Alternatively, tandem dimeric versions of FPs, in which two FP protomers of a dimeric FP are fused together using a flexible linker, and heterotetrameric FP tagging, in which a protein fused to a protomer of a tetrameric FP is coexpressed with an excess of a free non-fluorescent tetrameric FP mutant (8), have been used as protein tags. These FPs behave as pseudomonomers, but they are twofold–fourfold larger and may therefore interfere with the correct localizations of some fusions, such as those of tubulin and histones (54).

Considerations for specific applications—The fluorescence of FPs depends on pH and thus may vary in the physiological context of a cell. FPs with pK_a values of 5–6 are

compatible with studying proteins in the cytosol. In contrast, studying protein fusions in acidic organelles such as late endosomes and lysosomes requires probes with pK_a values of 4 or less.

Most photocontrollable FPs are activated by violet light, which can cause phototoxic effects in living cells (59). These effects include changes in cell shapes, DNA damage, and subsequent apoptosis. Still, the typical light intensities used in ensemble and single-molecule superresolution imaging with photocontrollable FPs are rather low. Photocontrollable proteins that can be photoswitched and imaged with long-wavelength light, such as photoswitchable monomeric orange fluorescent protein (PSmOrange) (80) and PSmOrange2 (79), should be considered for live-cell experiments.

Comparison of Superresolution Techniques

Current implementations of both single-molecule localization PALM and ensemble RESOLFT techniques use similar ranges of light intensities of 1–100 kW/cm^2. Arguably, RESOLFT may use a lower total light dose per live cell because this technique uses point-scanning, in contrast to PALM, in which the entire imaged area is irradiated during recording.

Compared with patterned illumination approaches, PALM is easier to implement technically. In addition to commercially available microscopes, custom-built systems can be designed (23, 52), and although postacquisition processing is required, many software programs are available to do so (52). The setup for patterned illumination microscopy is more challenging than that of PALM, but image acquisition is easier and requires less postacquisition processing.

Because of the low signal-to-background ratio in a highly absorbing, autofluorescing, and scattering background, imaging of thick biological samples is challenging for both PALM and RESOLFT approaches, especially for PALM. Several techniques have been introduced to permit single-molecule localization in three dimensions, including a biplane fluorescence PALM (47), a 3D interferometric PALM (iPALM) (71), an astigmatism-based 3D stochastic optical reconstruction microscopy (42), and a 3D PALM with two-photon illumination (86). The higher signal-to-background ratio due to imaging of an ensemble of molecules and the possibility of combining a superresolution technique with a confocal setup make RESOLFT promising for applications in relatively thick samples (25).

Superresolution imaging of dynamic processes always includes trade-offs between spatial and temporal resolution. The relatively slow acquisition speed was a limitation in the original implementation of PALM. This parameter has been improved in recent PALMIRA (18), s-PALM (19) and pcSOFI (16) techniques, and by using specific algorithms for scientific complementary metal–oxide–semiconductor cameras (44). There have also been advancements in the acquisition speeds of ensemble-based techniques. Specifically, the parallelized RESOLFT has enabled much faster image acquisition, reaching acquisition times of less than 2 seconds for the 100 μm × 120 μm field of view (10).

In contrast to ensemble imaging, single-molecule localization techniques are more suitable for quantitative studies, as they image individual molecules, which can be counted. In practice, however, blinking of fluorescent molecules interferes with counting them. Recently, several quantitative approaches have been reported that account for blinking using statistical pair correlation analysis (64), optimal spatial- and temporal-threshold–based grouping algorithms (61), and kinetic modeling (5, 50).

Both ensemble and single-molecule approaches allow researchers to use multicolor imaging, owing to the availability of a variety of spectrally resolvable photocontrollable FPs (16, 70, 75, 76). Overall, PALM and similar approaches utilizing photocontrollable FPs are widely used techniques, whereas patterned illumination methods utilizing rsFPs, including RESOLFT and nonlinear structured illumination, are currently used by a handful of labs but hold great potential for the future.

MODERN PHOTOCONTROLLABLE FLUORESCENT PROTEINS

Photoactivatable Fluorescent Proteins (PAFPs)

PAFPs photoconvert into a green or red fluorescent state after being photoactivated in a dark state by violet light (Table 1). These proteins are widely used in PALM because of their high contrast after photoactivation, their photostability, and their high photon emission rate. Moreover, because PAFPs are dark before photoactivation, they are ideal for use in two-color PALM imaging experiments, in which two types of tagged proteins are imaged simultaneously.

Photoactivatable green fluorescent protein (PAGFP) (58) was the first reported PAFP and is currently still the only dark-to-green PAFP. For this reason, PAGFP has been widely used in two-color imaging experiments in combination with dark-to-red PAFPs.

Photoactivatable monomeric red fluorescent protein-1 (PAmRFP1) (83) was the first dark-to-red PAFP. Insights from its development led to further engineering and the development of modern dark-to-red PAFPs, such as PAmCherry1 (75), PATagRFP (76), and PAmKate (27). Both PAmCherry1 and PATagRFP have exceptionally high contrast after photoactivation (Table 1). In PALM experiments, PAmCherry1 performs similarly to the photoswitchable FP tdEosFP (75). The recently developed dark-to-red PAFP, PATagRFP, has several characteristics that make it superior to other PAFPs in PALM applications. For example, its high photostability at the single-molecule level permits imaging of the same molecule through many frames, making PATagRFP an optimal choice for molecule tracking in single-particle-tracking PALM (sptPALM) (43) experiments. PATagRFP also exhibits a higher photon emission rate (i.e., more photons are detected per frame) than do other PAFPs, meaning that individual molecules can be more precisely localized in each frame.

PAmKate (48) is the most far-red shifted PAFP. Its photoactivation contrast is lower than that of PAmCherry1 or PATagRFP owing to its higher background noise at the single-molecule level. Because of its far-red shifted emission, PAmKate has been successfully used in three-color PALM imaging (27). The potential limitation of PAmKate is that its photoactivation contrast decreases over time after protein expression.

Photoswitchable Fluorescent Proteins (PSFPs)

PSFPs photoswitch from one fluorescent state into another in response to violet or blue-green light. This class of FPs includes (*a*) the cyan-to-green proteins, photoswitchable cyan fluorescent protein (PSCFP) and PSCFP2, (*b*) green-to-red Kaede-like proteins, (*c*) green-to-red IrisFP-like proteins, and (*d*) the orange-to-far-red proteins, PSmOrange and PSmOrange2.

The cyan-to-green proteins PSCFP (11) and enhanced PSCFP2 (13) are photoswitched by violet light. PSCFP2 photoswitches with a high contrast, although the brightness of the activated state is relatively low. Although PSCFP2 is inferior to green-to-red EosFP and its derivatives in terms of the number of photons emitted per molecule and in its photoactivation contrast, PSCFP2 has been successfully used with EosFP in two-color PALM imaging (70).

Green-to-red Kaede-like PSFPs share a common photoconversion mechanism and therefore can be considered as a group. All of these FPs are characterized by high brightness and high photoconversion contrast. Although it has been difficult to engineer monomeric Kaede-like FPs from their natural tetrameric precursors and to transfer the Kaede-like phenotype into monomeric FPs, the payoff has been substantial. Several modern, monomeric Kaede-like PSFPs have been developed, including mEos2 (54), mEos3.2 (87), Dendra2 (11, 28), mKikGR (31), mClavGR2 (39), and a mutant of mClavGR, mMaple (53). These molecules are among the best available PSFPs for techniques based on single-molecule localization (Table 1).

An early monomeric version of EosFP, called mEosFP, showed limited applicability owing to its inefficient folding at physiological temperatures. Instead, an efficiently maturing tandem dimeric version, tdEosFP (84), is now used in superresolution imaging (51, 69). However, the tandem dimeric tag performs poorly in many fusions because it forms filamentous structures in some intracellular environments (54). The development of monomeric mEos2 solved this problem: mEos2 retained the high contrast and high photon budget of its parent, EosFP, but showed only a weak tendency to dimerize and cause protein aggregation. The recently reported mEos3.1 and mEos3.2 are even better at avoiding dimerization and aggregation (87).

Green-to-red PSFPs Dendra (28), enhanced Dendra2 (13), and mKikGR (31) are valuable alternatives to mEos2. Dendra2 in particular is more monomeric than mEos2 and provides comparable localization precision (Table 1). Under PALM illumination conditions, Dendra2 photobleaches faster but blinks severalfold less than does mEos2 (50). Monomeric mKikGR also shows high performance in single-molecule imaging (31). In addition, a green-to-red PSFP called mClavGR2 (39), as well as its derivative mMaple, performs well in single-molecule superresolution imaging experiments, although these proteins lack notable advantages over mEos2 (53).

IrisFP (derived from EosFP) (1), monomeric mIrisFP (21), and NijiFP (derived from Dendra2) (2) all combine properties of irreversible and reversible photoswitching in a single protein. Similarly to Kaede-like PSFPs, mIrisFP and NijiFP can be irreversibly

photoswitched from green-to-red under irradiation with violet light. Illumination of an initial green form with either 488-nm or low-intensity violet light causes reversible switching of the green form off or on, respectively. The red form of these proteins can also be reversibly switched on by 440-nm light and off by 532-nm light. This complex photobehavior has enabled the use of mIrisFP in experiments combining sub–diffraction resolution imaging with pulse-chase selective photolabeling to study the dynamics, formation and disassembly of protein complexes (21).

The orange-to-far-red proteins PSmOrange (80) and PSmOrange2 (79) can be photoswitched with blue-green light. Interestingly, the far-red state of these PSFPs exhibits the most red-shifted excitation among all GFP-like FPs. PSmOrange and PSmOrange2 have demonstrated good performance in PALM (79, 80). PSmOrange2 has the blue-shifted photoswitching action spectrum, severalfold higher photoactivation contrast, and approximately tenfold faster photoactivation rate than PSmOrange. The potential limitation of both probes is that their photoswitching efficiency and kinetics depend on the redox environment. The spectral properties of both proteins should allow multicolor superresolution imaging with other PAFPs, including PAGFP and PSCFP2.

Reversibly Photoswitchable FPs (rsFPs)

rsFPs photoswitch between two states in response to activating light. In addition to photoswitching, rsFPs can spontaneously relax to their steady state with a relaxation half-time that varies from minutes to hours and that depends on temperature (Table 2) (12). These proteins are useful in both single molecule–based and ensemble–based superresolution techniques, although the rsFP requirements for use in these two types of techniques differ. In PALM experiments, rsFPs that have slow switching kinetics and that produce a large number of photons per cycle are desirable in order to provide high localization precision (55). In RESOLFT experiments, however, rsFPs with high fatigue resistance and faster switching kinetics are ideal (26, 74). Modern rsFPs exhibit one or more of these properties and include the following: (*a*) green Dronpa, its derivatives, and proteins with similar properties; (*b*) green-yellow Dreiklang for which the photoswitching light is decoupled from excitation; (*c*) green reversibly switchable enhanced GFP (rsEGFP) and its mutants; (*d*) red rsCherries; and (*e*) red rsTagRFP (Table 1).

Dronpa, which is bright and has relatively high photoswitching contrast, was the first widely used monomeric rsFP (3). Initially, Dronpa exhibits green fluorescence in response to excitation by blue light. High-intensity blue light then switches Dronpa off, and violet light turns the protein back on. This type of photobehavior, in which the switching off occurs at the fluorescence excitation wavelength, is termed negative switching. Dronpa has different absorbance spectra when in the on state versus the off state. This phenomenon is called photochromism. Although early studies demonstrated RESOLFT with Dronpa (15), its applicability to this technique is limited because of suboptimal switching kinetics and low fatigue resistance. Dronpa has been successfully applied to single-molecule localization techniques (9, 30, 70), and Dronpa mutants with fast switching kinetics, including rsFastlime (74) and Dronpa3 (19), have been utilized in PALMIRA and s-PALM. rsFPs with slow switching kinetics are likely to be useful in these techniques because they emit more

photons per cycle and thus can be localized with the higher precision (55). The recently developed mGeosM demonstrated a severalfold slower half-time for switching off, resulting in a higher localization precision than that of Dronpa and comparable to that of PAmCherry1 (9).

Several Dronpa mutants with distinct switching phenotypes have been developed. One of these mutants, bsDronpa, has absorbance and excitation spectra that are broader and blue-shifted compared to those of Dronpa (4). Similar to Dronpa, bsDronpa is switched on by violet light and switched off by blue light. Unlike Dronpa, however, it can be efficiently excited by both blue and violet light. Another Dronpa mutant, called Padron, has switching behavior antagonistic to Dronpa (4). Blue light switches Padron on and excites fluorescence, whereas violet light switches the protein off. This type of photoswitching behavior, when an rsFP undergoes off-on switching at fluorescence excitation wavelengths, is termed positive switching. Although they are useful in monochromatic multilabel confocal microscopy, none of the Dronpa mutants described above demonstrates substantial advantages over parental Dronpa in superresolution imaging. Moreover, rsFPs with positive switching are not readily applicable to PALM because activating a small subset of distantly located fluorescent molecules is difficult when the excitation light also switches them on.

Green-yellow Dreiklang, which is derived from the yellow FP Citrine, is the only reported rsFP whose fluorescence excitation is decoupled from photoswitching (7). Irradiation at 515 nm (near the excitation maximum) does not switch Dreiklang on; rather, illumination with 365-nm light switches the protein on, and illumination with 405-nm light switches it off. The switching phenotype of Dreiklang makes it possible to control the length and probability of a photoswitching cycle. By adjusting the irradiation time and the power of 355-nm and 405-nm lasers, researchers were able to image and localize individual molecules to within 15 nm. Dreiklang was also used in RESOLFT studies, in which a high resolution of 35 nm was achieved as a result of the protein’s high fatigue resistance and fast switching rate (Table 2). However, Dreiklang has several drawbacks. First, its switching properties are highly dependent on temperature, and fatigue resistance decreases at higher temperatures. Second, Dreiklang exhibits very fast spontaneous recovery from the off state at 37°C. Finally, switching requires UV light, which affects cell viability and can induce changes in cell morphology (7).

The recently reported reversibly switchable enhanced GFP (rsEGFP) (25) and rsEGFP2 (26) can be reversibly switched on and off by 405-nm light and 491-nm light, respectively. They exhibit properties that are advantageous for RESOLFT, including substantially higher fatigue resistance and faster switching kinetics than those of Dronpa (Table 2). A resolution of less than 40 nm was achieved in live cells using RESOLFT with rsEGFP (25). Still, the rsEGFP has relatively slow switching kinetics for use in point-scanning RESOLFT, resulting in an acquisition time of approximately 1 hour to record a typical image. The rsEGFP mutant, rsEGFP2, exhibits severalfold faster switching-off kinetics at low intensities of irradiating light, enabling 25–250-fold faster image recording (26). However, the resolution achieved using rsEGFP2 (50–90 nm) is lower than that obtained using rsEGFP because the shorter imaging cycle leads to a lower signal-to-background ratio. rsEGFP2 has the lower photoswitching contrast than does rsEGFP. An rsEGFP/N205S

mutant that switches off severalfold slower than rsEGFP and that emits twice more photons per cycle was used successfully in parallelized RESOLFT (10). Slow-switching rsFPs have advantages in fast-acquisition imaging such as parallelized RESOLFT because they emit large numbers of photons per cycle and therefore have higher signal-to-background ratios.

The first reported monomeric red rsFPs are the negative-switching rsCherryRev and the positive-switching rsCherry (73). Both proteins have low brightness and photoswitching contrast in ensemble. However, at the single-molecule level, some rsCherryRev and rsCherry molecules display tenfold higher brightness, which is comparable to the molecular brightness of their parent protein, mCherry. This phenomenon has enabled the use of rsCherryRev in PALMIRA (73). The difference in ensemble and single-molecule characteristics may be caused by competing transitions into other nonfluorescent states. Other limitations of these rsFPs are their relatively fast switching-off kinetics; low contrast; and complex photoswitching behavior, which includes changes in the contrast and fluorescence intensity that depend on the number of switching cycles the protein has undergone.

The recently engineered negative-switching red rsFP rsTagRFP (78) does not have the drawbacks of rsCherryRev. rsTagRFP can be switched on by yellow light and switched off by blue light. In contrast to rsCherry and rsCherryRev, its absorbance spectra profile changes upon photoswitching. rsTagRFP has a high ensemble brightness and a high photoswitching contrast, similar to those of the green rsFP Dronpa. The spectral and optimized photophysical properties of rsTagRFP have enabled its use with Dronpa in two-color pcSOFI (16). rsTagRFP should also be useful in two-color PALMIRA experiments, but its fatigue resistance makes it suboptimal for RESOLFT.

APPLICATIONS OF SUPERRESOLUTION MICROSCOPY USING PHOTOCONTROLLABLE FLUORESCENT PROTEINS

The success of PALM and related single molecule–based imaging techniques depends heavily on data processing and image reconstruction techniques. Various statistical and computational techniques have been developed for optimal detection of single molecules in crowded biological environments. The initial PALM superresolution studies utilized localization algorithms based on fitting of a single emitter profile within a diffraction-limited spot (6). However, these algorithms often led to discarding a fraction of the data when this condition was not satisfied, resulting in decreased sampling density. Recent developments in localization algorithms have readdressed this situation by allowing precise localization of multiple single-molecule emitters within a diffraction-limited spot (14, 40, 45, 72, 88). Depending on the data acquisition and processing algorithms employed for the experiment, the output can report different attributes of single-molecule organization and dynamics. Here we focus on the rationale and operational principles of some recent PALM approaches and highlight specific examples that underscore the versatility of these techniques.

Although it is not as developed as PALM, RESOLFT has already advanced superresolution microscopy. In contrast to single-molecule localization techniques, RESOLFT provides

superresolution images practically in real time, similar to confocal microscopy. We discuss several RESOLFT applications that have become possible as a result of recent progress in designing rsFPs and microscopy instrumentation.

Overall, improvements in the techniques used to analyze single-molecule statistics and spatial organization in PALM and in the implementation of hardware approaches in RESOLFT have transformed these superresolution microscopy methods into powerful tools for garnering key insights about protein organization, protein dynamics, and the fine structural details of cellular architecture.

Spatial Relationship Between Single Molecules

Dynamic clustering of protein molecules is a common mechanism for modulating processes like cell signaling, cell migration, and membrane trafficking. In recent years, it has become increasingly clear that such clustering often takes place within morphologically featureless areas of the cell. This is especially true for protein organization in mammalian cell membranes, manifested by the presence of membrane nanodomains with distinct protein compositions and by clusters of cell surface receptors held together by protein–protein and protein–lipid interactions. Understanding the mechanisms underlying the biogenesis of such protein clusters and how they regulate cellular processes is a key focus in biology. To achieve such an understanding, it is necessary to elucidate the protein content, nanoscale spatial organization, and dynamics of proteins within these molecular assemblies, as well as to monitor how such properties change during physiological processes. Until recently, this information has eluded scientists because of the paucity of biophysical techniques that can study nanoscale organization in a native biological context.

The development of PALM and other single-molecule techniques promises to furnish insights about the nanoscale spatial configuration of proteins because these techniques are able to produce high-density molecular localizations of thousands of specifically labeled proteins, independent of their presence in morphologically distinct structures. The analysis of this data provides unprecedented opportunities to detect and characterize the nanoscale spatial configuration of proteins within clusters. Furthermore, comparing the physical properties of these clusters can provide insights about how such organization is modulated during specific biological processes.

The extraction of quantitative information about protein organization from these superresolution data sets is not straightforward because of blinking, a phenomenon in which a single fluorescing molecule appears in multiple image frames punctuated by variable time periods (64, 65). If not taken into account, blinking can manifest as spurious clustering of proteins. Recognition of this problem has led to the development of statistical techniques to extract the actual spatial organization of proteins submerged in the cluster of localizations from multiple appearances. One of these approaches uses pair-correlation analysis in conjunction with prior knowledge about the spatial distribution of localizations arising from the same molecule (64). This algorithm, termed pair-correlation PALM, enables the detection of protein clusters and the estimation of physical parameters such as their size, protein number, and protein density. The technique was used to characterize clusters of signaling molecules such as Lat and Lyn, glycophosphatidylinositol (GPI)-anchored protein,

and a viral envelope protein (Figure 4*a*). In recent years, several other statistical techniques have been reported for evaluating the total number of proteins present in a superresolution data set (5, 50, 56), a critical parameter for proper analysis of the spatial organization of proteins. Cluster analysis algorithms, alone or in conjunction with such statistical approaches, have been used to characterize the spatial relationship of the transferrin receptor within endocytic pits (75), the organizational plasticity of asialoglycoprotein receptors on the plasma membrane (61), and the dynamic clustering of various signaling receptors and accessory proteins (68, 85). These studies underscore how advances in statistical techniques have allowed researchers to access the information within PALM data sets, helping to unravel the intricate spatial relationships that dictate the functional properties of biomolecules.

Structural Details of Molecular Assembly and Nanowriting

Apart from providing details about the relative positioning of single molecules, the large number of single-molecule positions furnished by PALM can also be used to reconstruct subcellular structures in a pointillistic fashion. Such high-resolution pointillistic depictions enable the study of closely spaced cellular structures, including the cytoskeleton, synaptic junctions, nuclear pores, cellular junctions, and adhesions. The localization of multiple proteins and their correlation with electron microscopy have been used to provide additional structural context for high-resolution pointillistic reconstructions derived from PALM data sets. The utility of PALM for interrogating nanoscale cellular organization received a further boost with the development of 3D imaging modalities. Some of the highlights of the studies performed using a combination of these techniques include (*a*) elucidation of the layered arrangement of different proteins within focal adhesions by 3D iPALM (48) (Figure 4*b*), (*b*) visualization of the spatial association between a mitochondrial nucleoid and a mitochondrial matrix protein (49), (*c*) delineation of the molecular details of aquaporin complex assembly on a cell membrane (62), and (*d*) description of bacterial chemotaxis and receptor clustering on the basis of self-organization principles (24).

RESOLFT imaging with rsFPs has allowed researchers to demonstrate nanowriting and data storage using biological molecules. Both repeated short-term data storage with the density of a DVD and permanent data writing became possible utilizing rsEGFP in RESOLFT (25). In the latter case, the data were written and read out with distances as small as 200 nm between individual bits; this density is fourfold denser than that achievable using regular light focusing.

Dynamics of Single Protein Molecules

PALM experiments performed with live cells are capable of providing insights about the dynamics of single protein molecules at nanoscopic spatial scales. Such single-molecule dynamics are exquisitely sensitive to the local microenvironment, and their motion reports the details of the nanoscale spatial heterogeneities that these molecules encounter as they navigate the cellular landscape. These spatial heterogeneities in turn play critical roles in organizing protein molecules and in determining the probability and duration of intermolecular interactions, thereby guiding the biological processes in which they

participate. Below, we discuss how PALM experimental protocols and data processing can be modified to furnish insights about these dynamic spatial heterogeneities.

In a PALM experiment with live cells, single fluorescing molecules are imaged multiple times during image acquisition. The localized positions of a molecule in successive image frames track its movement in space, and joining these discrete positions allows one to generate a high-resolution trajectory of the movement of the molecule. The sequential cycles of photoactivation or photoswitching, imaging, and photobleaching allow one to track sparsely distributed newly activated molecules as fluorescing molecules are removed from the visible pool of molecules by photobleaching. The sptPALM approach (51) allows one to track thousands of molecules in a single sample, enabling nearly exhaustive sampling of single-molecule dynamics over the entire spatial landscape. This technique provides a substantial advancement over traditional single-particle experiments in which the requirement for spatial separation of individual molecular tracks imposes a severe constraint on the number of trajectories that can be evaluated in a given experiment. Apart from exhaustive mapping of protein dynamics, sptPALM, by virtue of its vast sample size, also makes interrogation of infrequent intermolecular interactions possible.

Recent advances in the engineering of suitable PAFPs, such as PATagRFP, have enabled the implementation of two-color sptPALM to elucidate the nanoscale dynamics of several receptors correlated with the dynamics of clathrin-coated pits (76). sptPALM has also been used to interrogate the nanoscale spatial dynamics of the α-amino-3-hydroxy-5-methyl-4-isoxazolepropionic acid (AMPA) receptor in hippocampal dendrites (41). Through careful analysis of the sptPALM trajectories, the latter study concluded that a potential well generated by an assembly of binding receptors modulates the spatial organization of AMPA receptors (Figure 4*c*). These examples underscore how analysis of the diffusive behavior of a protein can provide insights about the mechanisms that modulate its dynamics and assembly.

Imaging of Living Cells

Even though the molecules localized in live-cell PALM experiments are in constant motion, their coordinates can be used to recreate a subcellular structure if the molecules are confined within it. In such a scenario, the successive coordinates of a molecule basically provide a sampling of different parts of the structure. Note, however, that such structural reconstruction is only possible if the time required for sufficient sampling is shorter than that of the dynamics of the organelle. This requirement limits the temporal resolution of this strategy to achieve a desired spatial resolution, allowing the study of only structures with dynamics of a few seconds or more.

In live-cell PALM, the image series is divided into subsets, each of which contains a certain number of successive image frames. The coordinates in each subset are combined separately to recreate a high–spatial resolution image of the structure, and each reconstruction gives a temporally updated snapshot of the structure. The collection of these reconstructed images therefore enables interrogation of the dynamics of molecular assemblies at high resolution. This approach has been utilized to observe the dynamics of focal adhesions in mammalian

cells (69) (Figure 4*d*) and the temporal evolution of signaling clusters during T-cell signaling (85).

RESOLFT microscopy, in addition to imaging static structures in live cells at a resolution of less than 40 nm (25), allows studies of cells by taking repeated images over time. Dynamic changes in actin filament organization have been followed in a dendrite within a living organotypic hippocampal slice at a resolution of less than 80 nm (25). The use of rsEGFP2 (26) with fast switching kinetics and parallelized imaging schemes, such as parallelized RESOLFT (10), helped to further increase the temporal resolution of time-lapse RESOLFT. Moreover, RESOLFT has been successfully used to document the dynamics of dendritic spines within hippocampal brain tissue (81) and those of neurites and filopodia of neuronal cells (10).

Acknowledgments

This work was supported by the grants GM073913, CA164468 and EB013571 from the National Institutes of Health. We would also like to acknowledge the many investigators whose important work and key contributions could not be cited here owing to space restrictions.

Glossary

FP	fluorescent protein
Diffraction limit	the minimal distance at which objects can be distinguished in light microscopy that is half of the wavelength of light according to Abbe’s law
Photocontrollable FP	any fluorescence protein whose excitation and/or emission can be modulated with light
PALM	photoactivated localization microscopy
RESOLFT	reversible saturatable optical fluorescence transition
Point-spread function (PSF)	the spatial intensity profile of light emitted by a point light source or object observed through an optical instrument such as a microscope
Localization precision	corresponds to standard deviation of the fitted Gaussian distribution and scales with inverse square root of the number of photons per molecule
PALMIRA	photoactivated localization microscopy with independently running acquisition
s-PALM	stroboscopic photoactivated localization microscopy
pcSOFI	photochromic stochastic optical fluctuation imaging
STED microscopy	stimulated emission depletion microscopy

Nyquist criterion	criterion stating that at least two data points per resolution unit must be recorded, meaning that labeling density limits the achievable resolution
Fatigue resistance	the number of on-off switching cycles a reversibly switching fluorophore can undergo before its fluorescence intensity decreases twofold
Molecular brightness	the number of photons emitted per second per molecule; saturatable parameter depending on excitation cross-section, quantum efficiency of emission, and excitation light intensity
Photoactivation contrast	the ratio between the fluorescence intensities in the photoswitched and original states
Photoactivatable fluorescent protein (PAFP)	fluorescent protein for which light irradiation irreversibly switches it from a dark state to a fluorescent state
Photostability	a measure characterizing the time required to irreversibly decrease the fluorescence intensity to half of its initial level
Photoswitchable fluorescent protein (PSFP)	fluorescent protein that is irreversibly photoswitchable from one fluorescent state to another
Photoswitching kinetics	a characteristic of the time at which the fluorescence signal changes twofold in the processes of turning fluorescence on or off
Reversibly switchable fluorescent protein (rsFP)	fluorescent protein that can be reversibly photoswitched between dark and fluorescent states

LITERATURE CITED

1. Adam V, Lelimousin M, Boehme S, Desfonds G, Nienhaus K, et al. Structural characterization of IrisFP, an optical highlighter undergoing multiple photo-induced transformations. Proc Natl Acad Sci USA. 2008; 105:18343–48. [PubMed: 19017808]
2. Adam V, Moeyaert B, David CC, Mizuno H, Lelimousin M, et al. Rational design of photo-convertible and biphotochromic fluorescent proteins for advanced microscopy applications. Chem Biol. 2011; 18:1241–51. [PubMed: 22035793]
3. Ando R, Mizuno H, Miyawaki A. Regulated fast nucleocytoplasmic shuttling observed by reversible protein highlighting. Science. 2004; 306:1370–73. [PubMed: 15550670]
4. Andresen M, Stiel AC, Folling J, Wenzel D, Schonle A, et al. Photoswitchable fluorescent proteins enable monochromatic multilabel imaging and dual color fluorescence nanoscopy. Nat Biotechnol. 2008; 26:1035–40. [PubMed: 18724362]
5. Annibale P, Vanni S, Scarselli M, Rothlisberger U, Radenovic A. Quantitative photo activated localization microscopy: unraveling the effects of photoblinking. PLoS ONE. 2011; 6:e22678. [PubMed: 21818365]
6. Betzig E, Patterson GH, Sougrat R, Lindwasser OW, Olenych S, et al. Imaging intracellular fluorescent proteins at nanometer resolution. Science. 2006; 313:1642–45. [PubMed: 16902090]

7. Brakemann T, Stiel AC, Weber G, Andresen M, Testa I, et al. A reversibly photoswitchable GFP-like protein with fluorescence excitation decoupled from switching. Nat Biotechnol. 2011; 29:942–47. Dreiklang performs well in both PALM and RESOLFT owing to its fatigue resistance and photoswitching decoupled from excitation. [PubMed: 21909082]
8. Bulina ME, Verkhusha VV, Staroverov DB, Chudakov DM, Lukyanov KA. Heterooligomeric tagging diminishes non-specific aggregation of target proteins fused with Anthozoa fluorescent proteins. Biochem J. 2003; 371:109–114. [PubMed: 12472468]
9. Chang H, Zhang M, Ji W, Chen J, Zhang Y, et al. A unique series of reversibly switchable fluorescent proteins with beneficial properties for various applications. Proc Natl Acad Sci USA. 2012; 109:4455–60. [PubMed: 22375034]
10. Chmyrov A, Keller J, Grotjohann T, Ratz M, d'Este E, et al. Nanoscopy with more than 100,000 'doughnuts'. Nat Methods. 2013; 10:737–40. Parallelized RESOLFT allows substantially faster image-acquisition speed than does point-scanning RESOLFT. [PubMed: 23832150]
11. Chudakov DM, Verkhusha VV, Staroverov DB, Souslova EA, Lukyanov S, Lukyanov KA. Photoswitchable cyan fluorescent protein for protein tracking. Nat Biotechnol. 2004; 22:1435–39. [PubMed: 15502815]
12. Chudakov DM, Matz MV, Lukyanov S, Lukyanov KA. Fluorescent proteins and their applications in imaging living cells and tissues. Physiol Rev. 2010; 90:1103–63. [PubMed: 20664080]
13. Chudakov DM, Lukyanov S, Lukyanov KA. Tracking intracellular protein movements using photoswitchable fluorescent proteins PS-CFP2 and Dendra2. Nat Protoc. 2007; 2:2024–32. [PubMed: 17703215]
14. Cox S, Rosten E, Monypenny J, Jovanovic-Talisman T, Burnette DT, et al. Bayesian localization microscopy reveals nanoscale podosome dynamics. Nat Methods. 2012; 9:195–200. [PubMed: 22138825]
15. Dedecker P, Hotta J, Flors C, Sliwa M, Uji-i H, et al. Subdiffraction imaging through the selective donut-mode depletion of thermally stable photoswitchable fluorophores: numerical analysis and application to the fluorescent protein Dronpa. J Am Chem Soc. 2007; 129:16132–41. [PubMed: 18047340]
16. Dedecker P, Mo GC, Dertinger T, Zhang J. Widely accessible method for superresolution fluorescence imaging of living systems. Proc Natl Acad Sci USA. 2012; 109:10909–14. [PubMed: 22711840]
17. Dickson RM, Cubitt AB, Tsien RY, Moerner WE. On/off blinking and switching behaviour of single molecules of green fluorescent protein. Nature. 1997; 388:355–58. [PubMed: 9237752]
18. Egner A, Geisler C, von Middendorff C, Bock H, Wenzel D, et al. Fluorescence nanoscopy in whole cells by asynchronous localization of photoswitching emitters. Biophys J. 2007; 93:3285–90. [PubMed: 17660318]
19. Flors C, Hotta J, Uji-i H, Dedecker P, Ando R, et al. A stroboscopic approach for fast photoactivation-localization microscopy with Dronpa mutants. J Am Chem Soc. 2007; 129:13970–71. [PubMed: 17956094]
20. Folling J, Bossi M, Bock H, Medda R, Wurm CA, et al. Fluorescence nanoscopy by ground-state depletion and single-molecule return. Nat Methods. 2008; 5:943–45. [PubMed: 18794861]
21. Fuchs J, Bohme S, Oswald F, Hedde PN, Krause M, et al. A photoactivatable marker protein for pulse-chase imaging with superresolution. Nat Methods. 2010; 7:627–30. mIrisFP undergoes green-to-red irreversible and dark-to-fluorescent reversible photoswitching, allowing pulse-chase imaging in two-color PALM. [PubMed: 20601949]
22. Gould TJ, Gunewardene MS, Gudheti MV, Verkhusha VV, Yin SR, et al. Nanoscale imaging of molecular positions and anisotropies. Nat Methods. 2008; 5:1027–30. [PubMed: 19011626]
23. Gould TJ, Verkhusha VV, Hess ST. Imaging biological structures with fluorescence photoactivation localization microscopy. Nat Protoc. 2009; 4:291–308. [PubMed: 19214181]
24. Greenfield D, McEvoy AL, Shroff H, Crooks GE, Wingreen NS, et al. Self-organization of the *Escherichia coli* chemotaxis network imaged with super-resolution light microscopy. PLoS Biol. 2009; 7:e1000137. [PubMed: 19547746]
25. Grotjohann T, Testa I, Leutenegger M, Bock H, Urban NT, et al. Diffraction-unlimited all-optical imaging and writing with a photochromic GFP. Nature. 2011; 478:204–8. Discusses the high

fatigue resistance of rsEGFP enables RESOLFT of live cells and provides a conceptual basis of RESOLFT. [PubMed: 21909116]

26. Grotjohann T, Testa I, Reuss M, Brakemann T, Eggeling C, et al. rsEGFP2 enables fast RESOLFT nanoscopy of living cells. eLIFE. 2012; 1:e00248. [PubMed: 23330067]
27. Gunewardene MS, Subach FV, Gould TJ, Penoncello GP, Gudheti MV, et al. Superresolution imaging of multiple fluorescent proteins with highly overlapping emission spectra in living cells. Biophys J. 2011; 101:1522–28. [PubMed: 21943434]
28. Gurskaya NG, Verkhusha VV, Shcheglov AS, Staroverov DB, Chepurnykh TV, et al. Engineering of a monomeric green-to-red photoactivatable fluorescent protein induced by blue light. Nat Biotechnol. 2006; 24:461–65. [PubMed: 16550175]
29. Gustafsson MG. Nonlinear structured-illumination microscopy: wide-field fluorescence imaging with theoretically unlimited resolution. Proc Natl Acad Sci USA. 2005; 102:13081–86. [PubMed: 16141335]
30. Habuchi S, Ando R, Dedecker P, Verheijen W, Mizuno H, et al. Reversible single-molecule photoswitching in the GFP-like fluorescent protein Dronpa. Proc Natl Acad Sci USA. 2005; 102:9511–16. [PubMed: 15972810]
31. Habuchi S, Tsutsui H, Kochaniak AB, Miyawaki A, van Oijen AM. mKikGR, a monomeric photoswitchable fluorescent protein. PLoS ONE. 2008; 3:e3944. [PubMed: 19079591]
32. Hell SW. Toward fluorescence nanoscopy. Nat Biotechnol. 2003; 21:1347–55. [PubMed: 14595362]
33. Hell SW. Far-field optical nanoscopy. Science. 2007; 316:1153–58. [PubMed: 17525330]
34. Hell SW. Microscopy and its focal switch. Nat Methods. 2009; 6:24–32. [PubMed: 19116611]
35. Hell SW, Wichmann J. Breaking the diffraction resolution limit by stimulated emission: stimulated-emission-depletion fluorescence microscopy. Opt Lett. 1994; 19:780–82. [PubMed: 19844443]
36. Hess ST, Girirajan TP, Mason MD. Ultra-high resolution imaging by fluorescence photoactivation localization microscopy. Biophys J. 2006; 91:4258–72. [PubMed: 16980368]
37. Hess ST, Gould TJ, Gudheti MV, Maas SA, Mills KD, Zimmerberg J. Dynamic clustered distribution of hemagglutinin resolved at 40 nm in living cell membranes discriminates between raft theories. Proc Natl Acad Sci USA. 2007; 104:17370–75. [PubMed: 17959773]
38. Hofmann M, Eggeling C, Jakobs S, Hell SW. Breaking the diffraction barrier in fluorescence microscopy at low light intensities by using reversibly photoswitchable proteins. Proc Natl Acad Sci USA. 2005; 102:17565–69. [PubMed: 16314572]
39. Hoi H, Shaner NC, Davidson MW, Cairo CW, Wang J, Campbell RE. A monomeric photoconvertible fluorescent protein for imaging of dynamic protein localization. J Mol Biol. 2010; 401:776–91. [PubMed: 20603133]
40. Holden SJ, Uphoff S, Kapanidis AN. DAOSTORM: an algorithm for high-density super-resolution microscopy. Nat Methods. 2011; 8:279–80. [PubMed: 21451515]
41. Hoze N, Nair D, Hosy E, Sieben C, Manley S, et al. Heterogeneity of AMPA receptor trafficking and molecular interactions revealed by superresolution analysis of live cell imaging. Proc Natl Acad Sci USA. 2012; 109:17052–57. [PubMed: 23035245]
42. Huang B, Wang W, Bates M, Zhuang X. Three-dimensional super-resolution imaging by stochastic optical reconstruction microscopy. Science. 2008; 319:810–13. [PubMed: 18174397]
43. Huang B, Babcock H, Zhuang X. Breaking the diffraction barrier: super-resolution imaging of cells. Cell. 2010; 143:1047–58. [PubMed: 21168201]
44. Huang F, Hartwich TM, Rivera-Molina FE, Lin Y, Duim WC, et al. Video-rate nanoscopy using sCMOS camera-specific single-molecule localization algorithms. Nat Methods. 2013; 10:653–58. [PubMed: 23708387]
45. Huang F, Schwartz SL, Byars JM, Lidke KA. Simultaneous multiple-emitter fitting for single molecule super-resolution imaging. Biomed Opt Express. 2011; 2:1377–93. [PubMed: 21559149]
46. Joo C, Balci H, Ishitsuka Y, Buranachai C, Ha T. Advances in single-molecule fluorescence methods for molecular biology. Annu Rev Biochem. 2008; 77:51–76. [PubMed: 18412538]

47. Juette MF, Gould TJ, Lessard MD, Mlodzianoski MJ, Nagpure BS, et al. Three-dimensional sub–100 nm resolution fluorescence microscopy of thick samples. Nat Methods. 2008; 5:527–29. [PubMed: 18469823]
48. Kanchanawong P, Shtengel G, Pasapera AM, Ramko EB, Davidson MW, et al. Nanoscale architecture of integrin-based cell adhesions. Nature. 2010; 468:580–84. [PubMed: 21107430]
49. Kopek BG, Shtengel G, Xu CS, Clayton DA, Hess HF. Correlative 3D superresolution fluorescence and electron microscopy reveal the relationship of mitochondrial nucleoids to membranes. Proc Natl Acad Sci USA. 2012; 109:6136–41. [PubMed: 22474357]
50. Lee SH, Shin JY, Lee A, Bustamante C. Counting single photoactivatable fluorescent molecules by photoactivated localization microscopy (PALM). Proc Natl Acad Sci USA. 2012; 109:17436–41. [PubMed: 23045631]
51. Manley S, Gillette JM, Patterson GH, Shroff H, Hess HF, et al. High-density mapping of single-molecule trajectories with photoactivated localization microscopy. Nat Methods. 2008; 5:155–57. [PubMed: 18193054]
52. Manley S, Gunzenhauser J, Olivier N. A starter kit for point-localization super-resolution imaging. Curr Opin Chem Biol. 2011; 15:813–21. [PubMed: 22119536]
53. McEvoy AL, Hoi H, Bates M, Platonova E, Cranfill PJ, et al. mMaple: a photoconvertible fluorescent protein for use in multiple imaging modalities. PLoS ONE. 2012; 7:e51314. [PubMed: 23240015]
54. McKinney SA, Murphy CS, Hazelwood KL, Davidson MW, Looger LL. A bright and photostable photoconvertible fluorescent protein. Nat Methods. 2009; 6:131–33. [PubMed: 19169260]
55. Mizuno H, Dedecker P, Ando R, Fukano T, Hofkens J, Miyawaki A. Higher resolution in localization microscopy by slower switching of a photochromic protein. Photochem Photobiol Sci. 2010; 9:239–48. [PubMed: 20126801]
56. Nieuwenhuizen RP, Lidke KA, Bates M, Puig DL, Grunwald D, et al. Measuring image resolution in optical nanoscopy. Nat Methods. 2013; 10:557–62. [PubMed: 23624665]
57. Patterson G, Davidson M, Manley S, Lippincott-Schwartz J. Superresolution imaging using single-molecule localization. Annu Rev Phys Chem. 2010; 61:345–67. [PubMed: 20055680]
58. Patterson GH, Lippincott-Schwartz J. A photoactivatable GFP for selective photolabeling of proteins and cells. Science. 2002; 297:1873–77. [PubMed: 12228718]
59. Post JN, Lidke KA, Rieger B, Arndt-Jovin DJ. One- and two-photon photoactivation of a paGFP-fusion protein in live *Drosophila* embryos. FEBS Lett. 2005; 579:325–30. [PubMed: 15642339]
60. Rego EH, Shao L, Macklin JJ, Winoto L, Johansson GA, et al. Nonlinear structured-illumination microscopy with a photoswitchable protein reveals cellular structures at 50-nm resolution. Proc Natl Acad Sci USA. 2012; 109:E135–43. [PubMed: 22160683]
61. Renz M, Daniels BR, Vamosi G, Arias IM, Lippincott-Schwartz J. Plasticity of the asialoglyco-protein receptor deciphered by ensemble FRET imaging and single-molecule counting PALM imaging. Proc Natl Acad Sci USA. 2012; 109:E2989–97. [PubMed: 23043115]
62. Rossi A, Moritz TJ, Ratelade J, Verkman AS. Super-resolution imaging of aquaporin-4 orthogonal arrays of particles in cell membranes. J Cell Sci. 2012; 125:4405–12. [PubMed: 22718347]
63. Rust MJ, Bates M, Zhuang X. Sub-diffraction-limit imaging by stochastic optical reconstruction microscopy (STORM). Nat Methods. 2006; 3:793–95. [PubMed: 16896339]
64. Sengupta P, Jovanovic-Talisman T, Skoko D, Renz M, Veatch SL, Lippincott-Schwartz J. Probing protein heterogeneity in the plasma membrane using PALM and pair correlation analysis. Nat Methods. 2011; 8:969–75. Combination of PALM with pair-correlation analysis enables studies of protein clusters, their size, their density, and their abundance in plasma membrane. [PubMed: 21926998]
65. Sengupta P, Lippincott-Schwartz J. Quantitative analysis of photoactivated localization microscopy (PALM) datasets using pair-correlation analysis. BioEssays. 2012; 34:396–405. [PubMed: 22447653]
66. Sengupta P, Van Engelenburg S, Lippincott-Schwartz J. Visualizing cell structure and function with point-localization superresolution imaging. Dev Cell. 2012; 23:1092–102. [PubMed: 23237943]
67. Shannon CE. Communication in the presence of noise. Proc IRE. 1949; 37:10–21.

68. Sherman E, Barr V, Manley S, Patterson G, Balagopalan L, et al. Functional nanoscale organization of signaling molecules downstream of the T cell antigen receptor. Immunity. 2011; 35:705–20. [PubMed: 22055681]
69. Shroff H, Galbraith CG, Galbraith JA, Betzig E. Live-cell photoactivated localization microscopy of nanoscale adhesion dynamics. Nat Methods. 2008; 5:417–23. [PubMed: 18408726]
70. Shroff H, Galbraith CG, Galbraith JA, White H, Gillette J, et al. Dual-color superresolution imaging of genetically expressed probes within individual adhesion complexes. Proc Natl Acad Sci USA. 2007; 104:20308–13. [PubMed: 18077327]
71. Shtengel G, Galbraith JA, Galbraith CG, Lippincott-Schwartz J, Gillette JM, et al. Interferometric fluorescent super-resolution microscopy resolves 3D cellular ultrastructure. Proc Natl Acad Sci USA. 2009; 106:3125–30. [PubMed: 19202073]
72. Smith CS, Joseph N, Rieger B, Lidke KA. Fast, single-molecule localization that achieves theoretically minimum uncertainty. Nat Methods. 2010; 7:373–75. [PubMed: 20364146]
73. Stiel AC, Andresen M, Bock H, Hilbert M, Schilde J, et al. Generation of monomeric reversibly switchable red fluorescent proteins for far-field fluorescence nanoscopy. Biophys J. 2008; 95:2989–97. [PubMed: 18658221]
74. Stiel AC, Trowitzsch S, Weber G, Andresen M, Eggeling C, et al. 1.8 A bright-state structure of the reversibly switchable fluorescent protein Dronpa guides the generation of fast switching variants. Biochem J. 2007; 402:35–42. [PubMed: 17117927]
75. Subach FV, Patterson GH, Manley S, Gillette JM, Lippincott-Schwartz J, Verkhusha VV. Photoactivatable mCherry for high-resolution two-color fluorescence microscopy. Nat Methods. 2009; 6:153–59. [PubMed: 19169259]
76. Subach FV, Patterson GH, Renz M, Lippincott-Schwartz J, Verkhusha VV. Bright monomeric photoactivatable red fluorescent protein for two-color super-resolution sptPALM of live cells. J Am Chem Soc. 2010; 132:6481–91. PATagRFP demonstrates advanced PALM properties and enables two-color single-particle tracking PALM together with PAGFP in live cells. [PubMed: 20394363]
77. Subach FV, Piatkevich KD, Verkhusha VV. Directed molecular evolution to design advanced red fluorescent proteins. Nat Methods. 2011; 8:1019–26. [PubMed: 22127219]
78. Subach FV, Zhang L, Gadella TW, Gurskaya NG, Lukyanov KA, Verkhusha VV. Red fluorescent protein with reversibly photoswitchable absorbance for photochromic FRET. Chem Biol. 2010; 17:745–55. rsTagRFP is characterized by high contrast and photochromism, allowing its use in various applications including two-color pcSOFI. [PubMed: 20659687]
79. Subach OM, Entenberg D, Condeelis JS, Verkhusha VV. A FRET-facilitated photoswitching using an orange fluorescent protein with the fast photoconversion kinetics. J Am Chem Soc. 2012; 134:14789–99. Orange-to-far-red PSmOrange2 is photoswitched by noncytotoxic blue-green light and awaits its application in multicolor PALM. [PubMed: 22900938]
80. Subach OM, Patterson GH, Ting LM, Wang Y, Condeelis JS, Verkhusha VV. A photoswitchable orange-to-far-red fluorescent protein, PSmOrange. Nat Methods. 2011; 8:771–77. [PubMed: 21804536]
81. Testa I, Urban NT, Jakobs S, Eggeling C, Willig KI, Hell SW. Nanoscopy of living brain slices with low light levels. Neuron. 2012; 75:992–1000. [PubMed: 22998868]
82. Thompson RE, Larson DR, Webb WW. Precise nanometer localization analysis for individual fluorescent probes. Biophys J. 2002; 82:2775–83. Derives the equation for a precision of localization of single molecules in fluorescence imaging. [PubMed: 11964263]
83. Verkhusha VV, Sorkin A. Conversion of the monomeric red fluorescent protein into a photoactivatable probe. Chem Biol. 2005; 12:279–85. [PubMed: 15797211]
84. Wiedenmann J, Ivanchenko S, Oswald F, Schmitt F, Rocker C, et al. EosFP, a fluorescent marker protein with UV-inducible green-to-red fluorescence conversion. Proc Natl Acad Sci USA. 2004; 101:15905–10. [PubMed: 15505211]
85. Williamson DJ, Owen DM, Rossy J, Magenau A, Wehrmann M, et al. Pre-existing clusters of the adaptor Lat do not participate in early T cell signaling events. Nat Immunol. 2011; 12:655–62. [PubMed: 21642986]

86. York AG, Ghitani A, Vaziri A, Davidson MW, Shroff H. Confined activation and subdiffractive localization enables whole-cell PALM with genetically expressed probes. Nat Methods. 2011; 8:327–33. [PubMed: 21317909]

87. Zhang M, Chang H, Zhang Y, Yu J, Wu L, et al. Rational design of true monomeric and bright photoactivatable fluorescent proteins. Nat Methods. 2012; 9:727–29. mEos3.1 and mEos3.2 are optimized for monomeric behavior, enabling PALM imaging of fused membrane proteins at high local density. [PubMed: 22581370]

88. Zhu L, Zhang W, Elnatan D, Huang B. Faster STORM using compressed sensing. Nat Methods. 2012; 9:721–23. [PubMed: 22522657]

SUMMARY POINTS

1. Photocontrollable FPs with high photon emission rates, large photon budgets, and high photoactivation contrast are optimal for superresolution imaging of single molecules. The chosen FP should also provide a high density of localized molecules.
2. The green-to-red PSFPs Dendra2, mEos2, mEos3.1, mKikGR, and mMaple have demonstrated good performance in PALM. The red PAFPs PAmCherry1 and PATagRFP provide high localization precision and can be combined with PAGFP for two-color imaging. The photocontrollable far-red PAmKate, cyan-to-green PSCFP2, and orange-to-far-red PSmOrange FPs present additional advantages for multicolor PALM.
3. Negative-switching rsFPs are applicable for PALM applications. The slower-switching rsFPs, such as Dronpa and rsTagRFP, emit more photons per cycle. However, the faster-switching rsFPs, including rsFastLime and Dronpa3, better suit PALMIRA and s-PALM.
4. rsFPs with high fatigue resistance are required for RESOLFT. The fatigue resistance of rsFPs depends on ensemble photostability and photoswitching kinetics. Currently, only green rsEGFP, its derivatives, and Dreiklang are suitable for RESOLFT imaging of mammalian cells.
5. Superresolution PALM and RESOLFT approaches with photocontrollable FPs have great potential to advance different areas of biology and medicine. These techniques have already enabled nanoscale imaging of subcellular organization and single biomolecules in various mammalian cells and tissues.

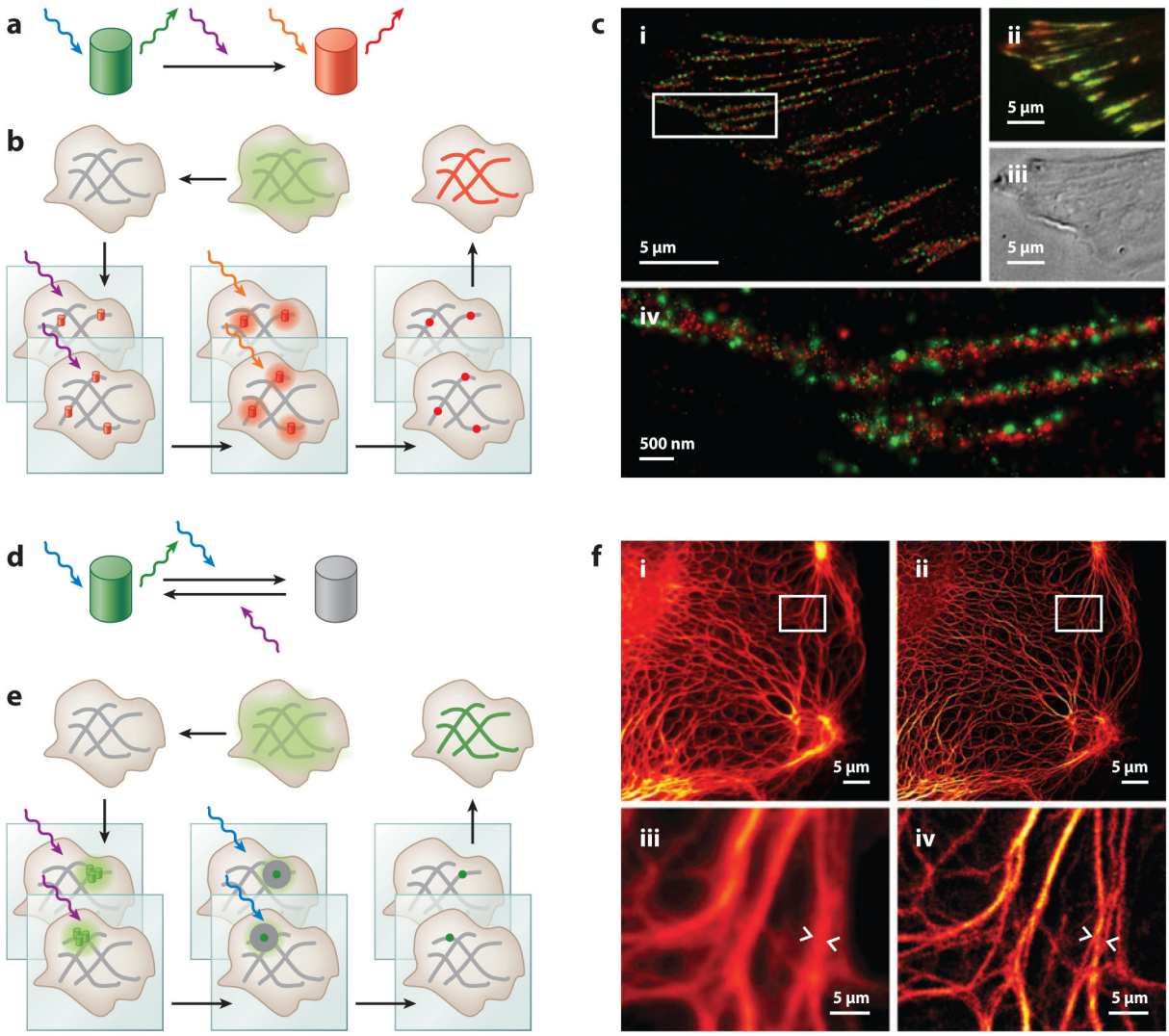

Figure 1.

Two major types of superresolution techniques using photocontrollable fluorescent proteins (FPs). (*a*) Phototransformations of a Kaede-like FP, an example of photocontrollable FPs used in photoactivated localization microscopy (PALM). (*b*) Schematic of the PALM approach. A small fraction of individual FP molecules are stochastically photoactivated with a low-intensity light, imaged, and photobleached. After repeating this process many times, the resulting images are processed to localize single molecules by finding the centroid positions in their point-spread functions. The final superresolution image is reconstructed by merging of all the localized single-molecule positions. (*c*) Example of a PALM image. (c_i) Dual-color PALM of paxillin-tdEosFP and zyxin-PSCFP2 fusions in HFF-1 cells. (c_{ii}) Same view as in *panel* c_i, imaged in a diffraction-limited mode. (c_{iii}) Differential interference contrast image of the same view as in panel c_i. (c_{iv}) Magnified view of the boxed region in panel c_i, showing little overlap of paxillin and zyxin. This overlap is not visible using diffraction-limited microscopy in total internal reflection fluorescence mode. Adapted from Reference 70, with permission from the *Proceedings of the National Academy of Sciences*.

 (*d*) Phototransformations of rsEGFP, an example of a photocontrollable FP used in reversible saturatable optical fluorescence transition (RESOLFT) approaches. (*e*) Schematic of a RESOLFT approach. The specimen is illuminated by three superimposed light beams: the switching-on laser, the excitation laser, and the collinear switching-off laser. The resulting doughnut-shaped area around the diffraction-limited excitation spot produces a sharpened effective fluorescent spot with a size of tens of nanometers in the lateral direction. A superresolution image is built by scanning these beams across the sample. (*f*) Example RESOLFT images. (f_i) Wide-field image of Ptk2 cells expressing keratin-rsEGFP/N205S fusion. (f_{ii}) Same view as in panel f_i, imaged in parallelized RESOLFT. (f_{iii}) Magnified view of the boxed region in panel f_i. (f_{iv}) Magnified view of the boxed region in panel f_{ii}. The intensity profiles of the regions between arrowheads were analyzed, and the experimentally determined full-width half maxima values corresponding to three filaments not resolvable in wide-field images (f_{iv}) were 77, 133, and 110 nm. Adapted from Reference 10, with permission from Nature Publishing Group.

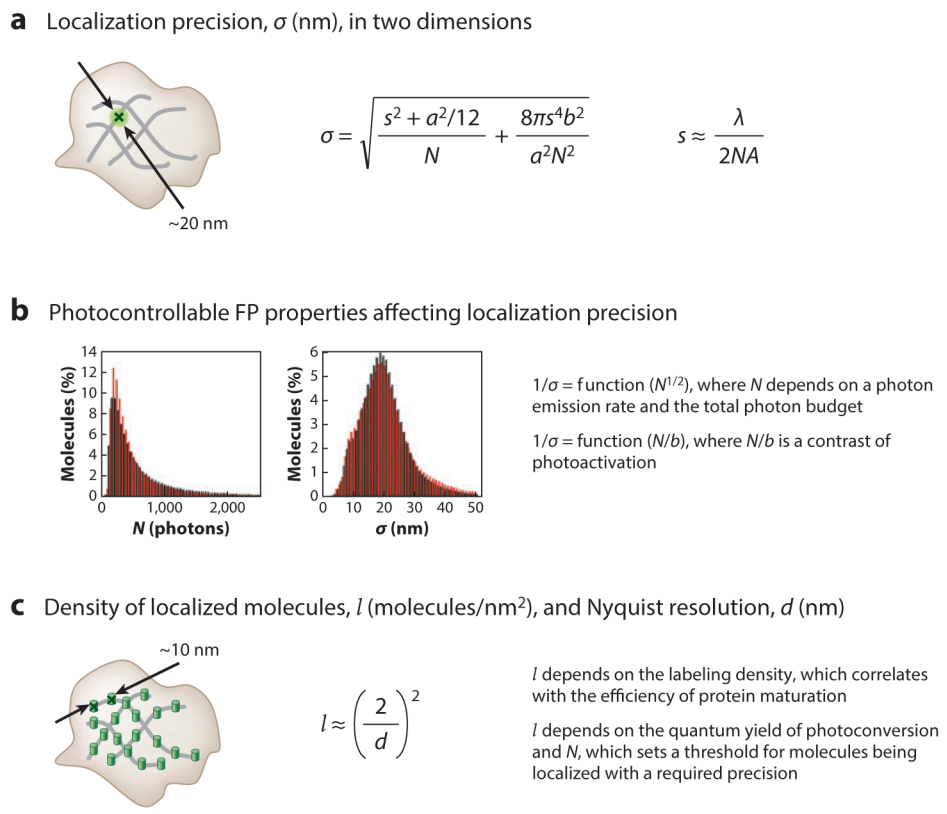

Figure 2.

Spatial resolution in photoactivated localization microscopy (PALM) and related techniques and parameters affecting it. (*a*) Spatial localization precision, σ (nm), in two dimensions. (*b*) Properties of photocontrollable fluorescent proteins (FPs) that affect localization precision. (*c*) Density of localized molecules, l (molecules/nm^2), and Nyquist resolution, d (nm). Abbreviations: a (nm), size of a pixel ($s > a$); b, background noise (number of photons collected from background in the spot being localized); λ (nm), wavelength; N, number of collected photons; NA, numerical aperture of the lens; s (nm), size of a diffraction-limited spot.

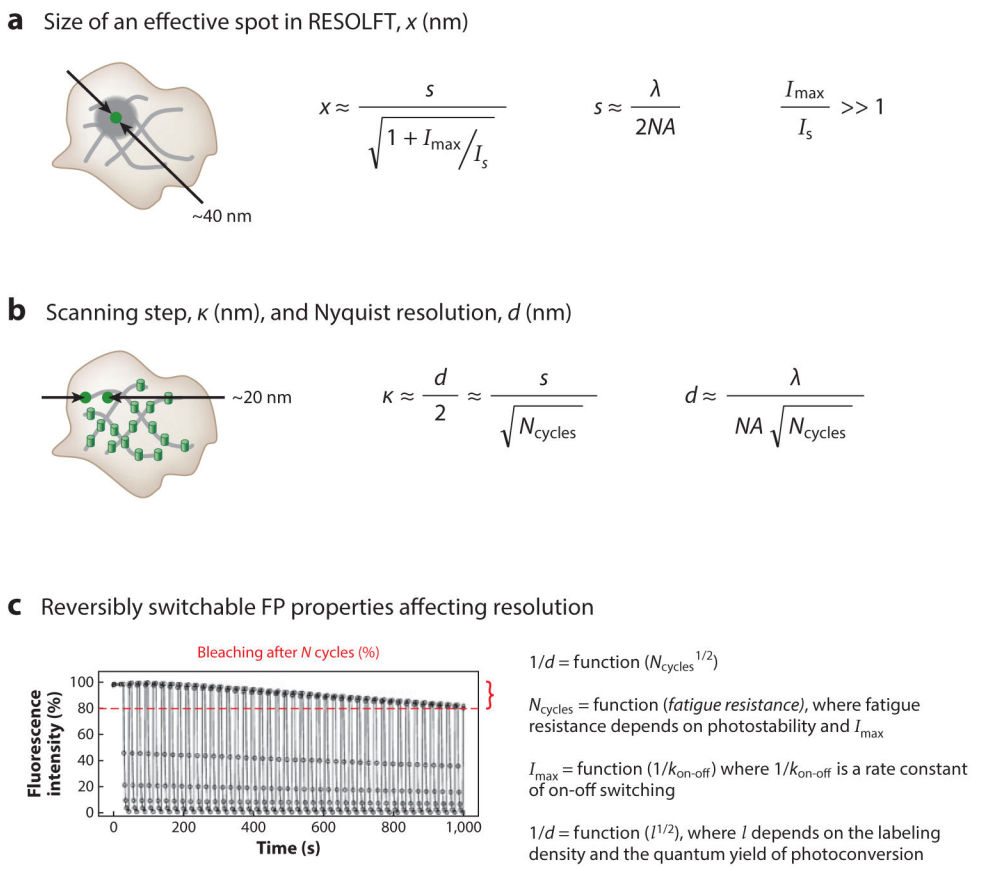

Figure 3.

Spatial resolution in reversible saturatable optical fluorescence transition (RESOLFT) and parameters of reversibly switchable fluorescent proteins (rsFPs) affecting this resolution. (*a*) Size of an effective spot in RESOLFT, x (nm). (*b*) Scanning step, κ (nm), and Nyquist resolution, d (nm). Abbreviations: I_{max} (W/cm^2), light intensity of the saturating doughnut-like RESOLFT beam; I_s (W/cm^2), light intensity at which the probability of changing the rsFP's state is 50%; l (molecules/nm^2), density of photoswitched rsFP molecules; λ (nm), wavelength; NA, numerical aperture of the lens; N_{cycles}, number of photoswitching cycles with a minimal loss of fluorescence intensity; s (nm), size of a diffraction limited spot.

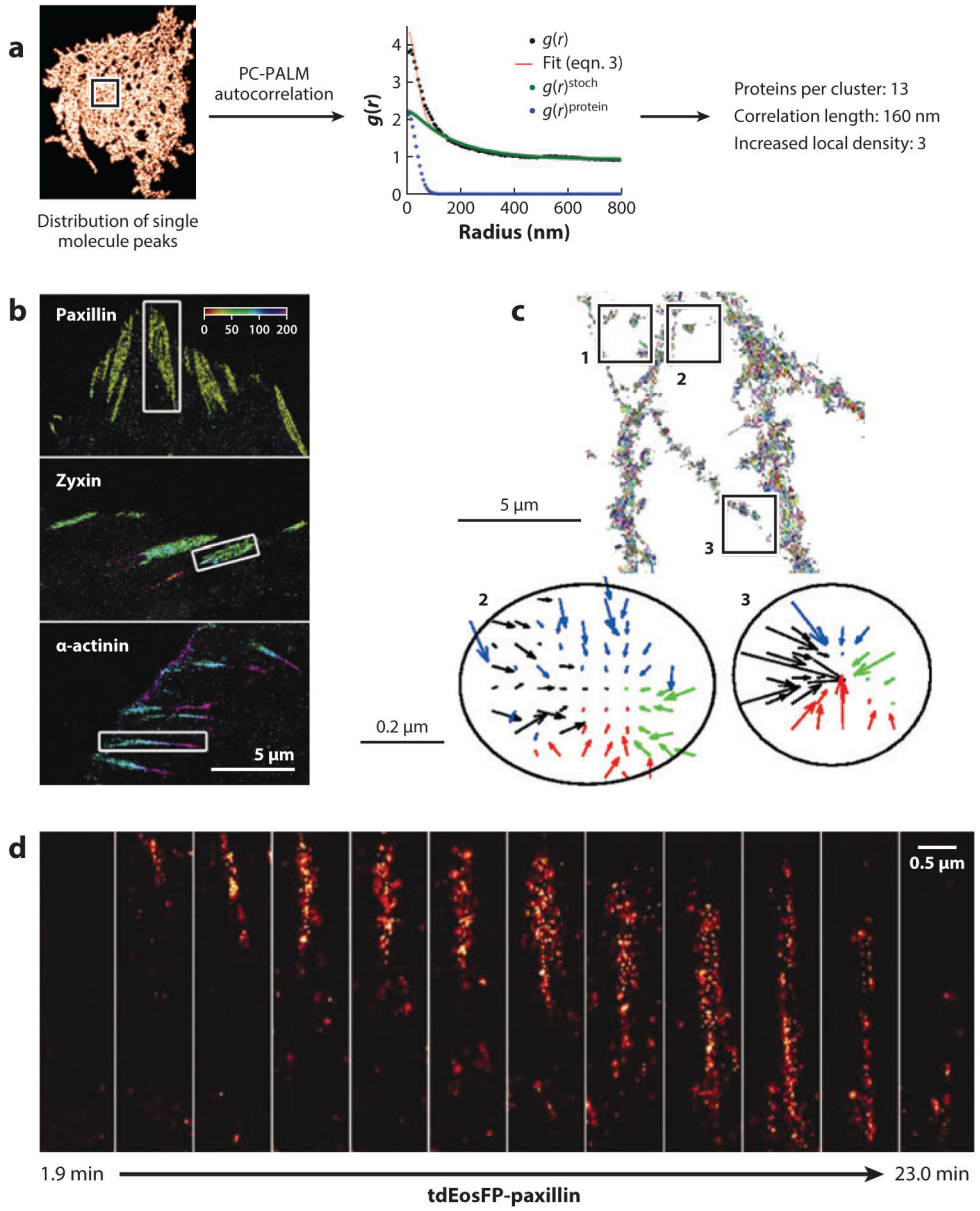

Figure 4.

Applications of photocontrollable fluorescent protein (FP)-based superresolution microscopy. (*a*) Workflow of pair-correlation photoactivated localization microscopy (PALM) analysis for detection and characterization of protein clusters. Rendered PALM image of photoactivatable green fluorescent protein (PAGFP)-tagged Lyn kinase expressed in COS-7 cells. Pair-correlation analysis of a subsection (*black box*) of the plasma membrane reveals clustered organization of Lyn. The actual correlation function of the protein molecules (*green circles*) is evaluated by the mathematical fitting (*red line*) of the measured correlation function (*black circles*). The correlation function due to blinking-induced multiple appearances of the same fluorescent molecule is represented by blue circles. Panel adapted from Reference 65 with permission from Wiley. (*b*) Use of

interferometric PALM (iPALM) for three-dimensional imaging of the nanoscale architecture of focal adhesion in mammalian cells. The iPALM reconstruction reveals the layered architecture of the focal adhesion; colors indicate the vertical distance (in nanometers) of the different focal adhesion proteins from the cover glass. Panel adapted from Reference 48 with permission from Nature Publishing Group. (*c*) Analysis of single-particle tracking PALM trajectories of α-amino-3-hydroxy-5-methyl-4-isoxazolepropionic acid (AMPA) receptor molecules in hippocampal dendrites shows that the receptors are organized into clusters by physical interactions with cooperative membrane binding sites. The local force fields constructed from an analysis of the single AMPA receptor dynamics converge to a single point, indicating direct molecular interaction between the receptor molecules and some of their binding partners. Three disjoint interacting potentials are shown (*bottom*) for the marked regions of molecular trajectories (*top*). Panel adapted from Reference 41 with permission from the *Proceedings of the National Academy of Sciences*. (*d*) Spatial dynamics and remodeling of focal adhesion depicted by an image series reconstructed using PALM of tdEosFP-paxillin. The image series documents the incorporation of paxillin into maturing focal adhesion. Panel adapted from Reference 69 with permission from Nature Publishing Group.

Table 1

Characteristics of modern monomeric photocontrollable fluorescent proteins

Protein	Excitation (absorbance) maximum (nm)	Emission maximum (nm)	Extinction coefficient (M^{-1} cm^{-1})	Quantum yield	Bright-ness[a]	pK_a	Photo-stability	Photo-activation contrast[b]	Photoactivation light wavelength (nm)	Maturation[c] half-time (min)	Localization precision σ in PALM (nm [i])	Reference
Photoactivatable Fluorescent Proteins (PAFPs)												
PAGFP	400	515	20,700	0.13	2.6	ND	ND	200	405	ND	~40 (37)	(58)
	504	517	17,400	0.79	13.7	6.3	Low					
PAmRFP1	(405)	ND	ND	ND	ND	ND	ND	70	405	ND	ND	(83)
	578	605	10,000	0.08	0.8	4.4	Medium					
PAmCherry1	(404)	ND	6,500	ND	ND	ND	ND	4,000	405	23	~10–15 (9), ~20 (75)	(75)
	564	595	18,000	0.46	8.3	6.3	Medium					
PATagRFP	(278)	ND	ND	ND	ND	ND	ND	>5,000	405	75	~20 (76)	(76)
	562	595	66,000	0.38	25	5.3	High					
PAmKate	(442)	ND	ND	ND	ND	ND	ND	100	405	19	~25–30 (27)	(27)
	586	628	25,000	0.18	4.5	5.6	High					
Photoswitchable Fluorescent Proteins (PSFPs)												
PSCFP2	400	470	43,000	0.20	8.6	4.3	ND	400	405	ND	~30 (70)	(11, 13)
	490	511	47,000	0.23	11	6.1	Low					
Dendra2	490	507	45,000	0.50	23	6.6	Medium	300	405 / 488	90	~10 (22), ~20 (54)	(13, 28)
	553	573	35,000	0.55	19	6.9	High					
tdEosFP (tandem dimer)	506	516	84,000	0.66	55	5.7	Medium	200	405	72	~10 (70), ~20–25 (51, 75)	(84)
	569	581	33,000	0.60	20	ND	High					
mEos2	506	519	56,000	0.84	47	5.6	Medium	~200[d]	405	<120	~10 (54)	(54)
	573	584	46,000	0.66	30	6.4	High					
mEos3.2	507	516	63,400	0.84	53	5.4	Medium	ND	405	<90[e]	~10 (87)	(87)
	572	580	32,200	0.55	18	5.8	High					
mKikGR	505	515	49,000	0.69	34	6.6	Low	400	405	ND	<15 (71)	(31)
	580	591	28,000	0.63	18	5.2	Medium					
mClavGR2	488	504	19,000	0.77	15	8.0	Low	~200[d]	405	<90[e]	<30 (87)	(39)

Protein	Excitation (absorbance) maximum (nm)	Emission maximum (nm)	Extinction coefficient (M^{-1} cm^{-1})	Quantum yield	Bright-ness[a]	pK_a	Photo-stability	Photo-activation contrast[b]	Photoactivation light wavelength (nm)		Maturation[c] half-time (min)	Localization precision σ in PALM (nm [i])	Reference
	566	583	32,000	0.53	17	7.3	Medium						
mMaple	489	505	15,000	0.74	11	8.2	High	~400[d]	405		<90[e]	ND	(53)
	566	583	30,000	0.56	17	7.3	High						
mIrisFP	(386)	ND	12,000	ND	ND	ND	ND	ND	405	405	> 14	~30–50 (21)	(21)
	486	516	47,000	0.54	25	5.4				473			
	(446)	ND	21,000	ND	ND	ND	ND			473		~20–40 (21)	
	546	578	33,000	0.59	19	7.6				561			
NijiFP	(~375)	ND	ND	ND	ND	ND	ND	ND	405	405	ND	~25 (2)	(2)
	469	507	41,100	0.64	26	7.0				488			
	(~440)	ND	ND	ND	ND	ND	High			440		~35 (2)	
	526	569	42,000	0.65	27	7.3				561			
PSmOrange	548	565	113,300	0.51	58	6.2	High	560	480	540	90	~45 (80)	(80)
	636	662	32,700	0.28	9.2	5.6	High						
PSmOrange2	546	561	51,000	0.61	31	6.6	Medium	680	480	540	210	~10–20 (79)	(79)
	619	651	18,900	0.38	7.2	5.4	High						
Reversibly Switchable Fluorescent Proteins (rsFPs)													
Dronpa	(392)	ND	ND	ND	ND	ND	ND	20	405		ND	~20 (18), ~30 (9)	(3)
	503	518	95,000	0.85	81	5.0	Low		488				
Dronpa3	ND	ND	ND	ND	ND	ND	ND	ND	405		ND	ND	(19)
	487	514	58,000	0.33	19	ND	ND		488				
rsFastLime	(384), (496)	ND	ND	ND	ND	ND	ND	~30– 50[f]	405		ND	~40 (18)	(74)
	496	518	39,100	0.77	30	ND	Medium		488				
Padron[g]	(505)	ND	ND	ND	ND	ND	ND	~20[f]	488		ND	ND	(4)
	(396), 503	522	43,000	0.64	28	ND	Medium		405				
bsDronpa	(385)	ND	ND	ND	ND	ND	ND	~20[f]	405		ND	ND	(4)
	460	504	45,000	0.50	23	ND	Medium		488				
mGeosM	(390)	ND	ND	ND	ND	ND	ND	20	405		ND	~15 (9)	(9)

Protein	Excitation (absorbance) maximum (nm)	Emission maximum (nm)	Extinction coefficient (M^{-1} cm^{-1})	Quantum yield	Bright-ness[a]	pK_a	Photo-stability	Photo-activation contrast[b]	Photoactivation light wavelength (nm)	Maturation[c] half-time (min)	Localization precision σ in PALM (nm [i])	Reference
	503	514	51,600	0.85	44	5.0	ND		488			
Dreiklang	(340), (511)	ND	ND	ND	ND	ND	ND	> 20	365	120	~15 (7)	(7)
	(412), 511	529	83,000	0.41	34	7.2	Medium		405			
rsEGFP	(396)	ND	ND	ND	ND	ND	ND	~30–50[f]	405	180	ND	(25)
	493	519	47,000	0.36	17	6.5	High		488			
rsEGFP2	(408)	ND	ND	ND	ND	ND	ND	~12– 15[f]	405	~20	ND	(26)
	478	503	61,300	0.30	18	5.8	High		488			
rsCherry	572	610	81,000	0.009	0.7	ND	ND	3[h]	550	ND	ND	(73, 78)
	572	610	80,000	0.02	1.6	6.0	Low		450			
rsCherryRev	572	608	41,800	0.0017	0.07	ND	ND	3[h]	450	42	ND	(73, 78)
	572	608	42,300	0.0051	0.22	5.5	Low		550			
rsTagRFP	440	585	15,300	0.0013	0.02	ND	ND	20	440	43	ND	(78)
	567	585	36,800	0.11	4	6.6	Medium		570			

Coloration of cells reflects excitation (or absorbance), fluorescnce, and photoconversion light for a fluorescent protein (FP); cells with gray backgrounds correspond to the dark (nonfluorescent) state. The upper row for each FP describes its parameters before photoconversion and the lower row describes its parameters after photoconversion. The complex photoswitching behavior of mIrisFP and NijiFP is described in the text. Maturation half-times are indicated for purified FPs.

Abbreviations: ND, not determined; PALM, photoactivated localization microscopy.

[a] A brightness in $(mM\ cm)^{-1}$ is determined as the product of extinction coefficient in $(M\ cm)^{-1}$ and quantum yield.

[b] An increase (fold) in fluorescence signal of the photoconverted state.

[c] Maturation process includes both protein folding and chromophore formation.

[d] Values are based on comparison with tsEosFP and mEos2.

[e] Values are based on comparison with Dendra2 and mEos2.

[f] Values are based on data for residual fluorescence in the off state reported in References 4, 25, and 26.

[g] Although monomeric at 37°C, Padron was shown to form dimers at 4°C (4).

[h] Data from Reference 78.

[i] The numbers were averaged to account for possible variability in biological samples expressing fluorescent proteins, their preparation, and imaging conditions.

Table 2

Specific properties of reversibly switchable fluorescent proteins related to their applicability to superresolution imaging

Protein	Residual signal in the off state (%)	Fatigue resistance (number of switching cycles to bleach to 50% of initial fluorescence)	Photoswitching kinetics		Relaxation half-time at room temperature (min)	Equilibrium state at room temperature (% of maximal fluorescence)	Reference
			On-to-off switching half-times (s); light power (W/cm^2)[a]	Off-to-on switching half-times (s); light power (W/cm^2)[a]			
Dronpa	~10	4	15.0; 0.045[b] (4)	0.12; 0.048[c] (4)	840	100	(4, 25, 78)
			0.016; 600[d] (25)	0.00005; 2,000 (25)			
			0.8; 0.4[g] (25)	0.6; 40[h] (25)			
rsFastlime	1–2	35	2.6; 0.045[b]	0.03; 0.048[c]	8	93	(4, 25)
Padron	15	16	0.06; 0.048[c]	5.6; 0.045[b]	150	5	(4, 25)
bsDronpa	10	~100	1.25; 0.045[b]	0.04; 0.048[c]	54	95	(4)
Dreiklang	1.4–15	160[e]	<1; 70[b]	~3; 0.7[f]	4	100	(7)
rsEGFP	1–2 (25) ~3–4 (26)	>500 ~1,100	0.001; 600[d]	0.00002; 2,000	23	100	(25, 26)
rsEGFP2	~7–8	~2,100	0.0004; 5,500[d]	<0.00004; 2,000	ND	100	(26)
rsCherryRev	>20 (25, 78)	>140 (78)	0.7; 4[i] (73)	0.105; 4[j] (73)	<0.5	8	(25, 73, 78)
			2.8; 5[k] (78)	0.0033; 10[l] (78)			
rsTagRFP	~5	>140	1.3; 5[k]	0.0017; 10[l]	65	30	(78)
			0.18; 4,900[m]	0.0028; 300[n]			

The fatigue resistance and residual fluorescence may vary depending on the sample preparation and experimental conditions, particularly the power of irradiating light. For example, the background for Dreiklang is 5–10% in bacterial streaks, whereas it is 1.4% in wide-field images of mammalian cells (7). The equilibrium state indicates the relative fluorescenece intensity achieved by a fluorescent protein after the relaxation in the darkness.

Abbreviation: ND, not determined.

[a]The wavelengths of switching light correspond to those shown in Table 1, with the exception of [d]491 nm, [g]390 nm, and [h]480 nm. The filter widths are [b]488/10 nm, [c]405/10 nm, [f] 365/25 nm, [g]390/40 nm, [h]480/40 nm, [i]550/20 nm, [j]450/20 nm, [k]570/30 nm, [l]436/20 nm, [m]570/5 nm, and [n]440/5 nm. [e]This value is temperature dependent: It decreases with an increase in temperature (7).